JCTC Journal of Chemical Theory and Computation

Article

pubs.acs.org/JCTC

Computational Chemistry Meets Experiments for Explaining the Behavior of Bibenzyl: A Thermochemical and Spectroscopic (Infrared, Raman, and NMR) Investigation

Camille Latouche and Vincenzo Barone*

Chemistry, Faculty of Science, Scuola normale Superiore di Pisa, Piazza dei Cavalieri 7, 56126 Pisa PI, Italy

Supporting Information

ABSTRACT: The structure, conformational behavior, and spectroscopic parameters of bibenzyl have been investigated by a computational protocol including proper treatment of anharmonic and hindered rotor contributions. Conventional hybrid functionals overstabilize the *anti* conformer while low-order post-Hartree−Fock (MP2) approaches strongly favor the *gauche* conformer. However, inclusion of semiempirical dispersion effects in density functionals or coupled cluster post-Hartree−Fock models agree in forecasting the simultaneous presence of both conformers in the gas phase with a slightly larger stability (0.7 kcal·mol^{-1}) of the *gauche* conformer. Addition of thermal and entropic effects finally leads to very close Gibbs free energies for both conformers and, thus, to a slight preference for the gauche form due to statistical factors (2 vs 1). The situation remains essentially the same in solution. On these grounds, perturbative vibrational computations including both electrical and mechanical anharmonicities lead to IR and Raman spectra in remarkable agreement with experiment. Full assignment of the IR spectra explains the presence of peaks from gauche or anti conformers. Comparison between computed and experimental Raman spectra confirms that both conformers are present in liquid phase, whereas the anti conformer seems to be preponderant in the solid state. Also computed NMR parameters are in good agreement with experiment.

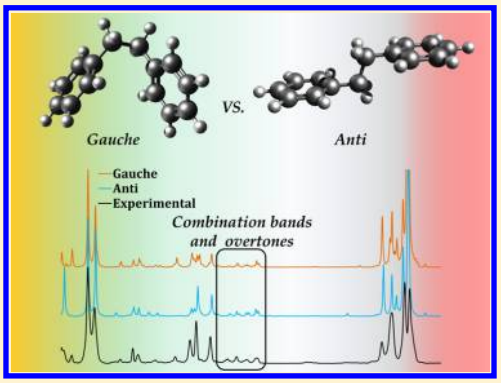

INTRODUCTION

In the field of conformational investigations, 1,2-diphenylethane (also known as dibenzyl or bibenzyl), abbreviated DPE, is one of the most targeted entities. Among nonrigid molecules, DPE and its derivatives have been extensively studied due to their interest for a large number of applications. For instance, the phytotoxic behavior of DPE derivatives in orchid (orchid bibenzyls gigantol) has exhibited a good potential concerning the development of a new class of herbicidal agents.[1] Other derivatives of the same family have been isolated as antiplatelet aggregation principles with efficient suppressive effects.[2,3] Together with their role in biotechnological applications,[4] molecules containing a bibenzyl moiety or a derivative are also crucial compounds in the synthesis of dyes, polymers, or resins.[5,6] Recently, a theoretical investigation has shown the role of bibenzyl concerning the reductive decomposition of [U(Tren^{TIPS})(CH$_2$Ph)]" to [U(Tren^{TIPS})] uranium complexes.[7]

As mentioned above, the conformational behavior of DPE has been widely investigated in the past decades, but both experimental and theoretical studies failed to give a definitive answer concerning the relative stabilities and, possibly, interconversion rates of the *anti* (antiperiplanar, Figure 1) and the *gauche* (synclinal) conformers.[8−11] In addition, some experimental evidences suggest that the environment of the molecule plays an important role in tuning its conformational preferences. Indeed, it has been reported that only the *anti* conformer is populated in the crystal,[12,13] (although the presence of the *gauche* conformer cannot be completely excluded[10]), whereas both conformers have been unequivocally detected when the molecule is in the liquid phase.[11]

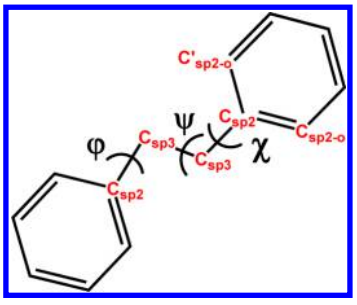

Figure 1. Bibenzyl sketch.

Recently, a joint experimental and theoretical study provided results accurate enough to characterize the *gauche* and *anti* conformers in the gas phase, especially in the far infrared region (FIR).[14] However, the anharmonic corrections computed by the authors led to an imaginary frequency casting doubts on the underlying perturbative vibrational treatment.[13] Furthermore, anharmonic corrections to IR intensities were not computed,

Received: October 21, 2014
Published: November 7, 2014

dx.doi.org/10.1021/ct500930b | J. Chem. Theory Comput. 2014, 10, 5586−5592

and this implies, for instance, that overtones and combination bands cannot be confidently assigned. In our opinion, a detailed characterization of the energetic profile along the soft internal degrees of freedom (essentially the two torsional angles around Csp^2-Csp^3 bonds and especially around the central Csp^3-Csp^3 bond; see Figure 1) is a mandatory prerequisite for any detailed spectroscopic characterization.

In view of the nonconclusive results obtained also in the most recent studies,[8,9] we have decided to perform a thorough investigation of the thermodynamic and kinetic aspects of this part of the potential energy surface (PES) including also anharmonic[15] and hindered rotor[16,17] contributions. Next, we will show that proper use of second order Vibrational Perturbation Theory (VPT2)[15] including symmetry constraints allows to characterize without any ambiguity the *anti* and *gauche* conformers as true energy minima (all positive vibrational frequencies at both harmonic and anharmonic levels). Only full account of both mechanical and electrical anharmonicity[18,19] allows to assign the whole IR and Raman spectra (including overtones and combination bands) and, by comparison with the experimental spectra available from the NIST database,[20] to detect bands due to different conformers. These results show that proper use of the most recent computational tools available for taking into account, when needed, anharmonic and hindered-rotation effects provide thermodynamic and spectroscopic results in quantitative agreement with experiment, thus allowing a more confident interpretation of the behavior of flexible molecules. Finally, we provide new results and explanations concerning bands in the mid-IR, together with full interpretation of Raman and NMR spectra. Ongoing implementation of all those tools in our user-friendly virtual multifrequency spectrometer (VMS)[21] and development of a new graphical user interface (VMS-Draw)[22] will allow, in the near future, such kind of direct comparisons between experimental and computed results also to non-specialists.

COMPUTATIONAL DETAILS

All calculations have been carried out with a locally modified version of the Gaussian suite of programs.[23] Most of the computations were performed by the B3LYP hybrid density functional,[24−26] in conjunction with the 6-31+G(d) basis set.[27]Additional computations have been performed using B3LYP, the double-hybrid B2PLYP functional,[28] MP2,[29−33] and CCSD(T)[34] approaches, in conjunction with the m-aug-cc-pVTZ basis set,[35,36] where *d* functions on hydrogens have been removed. Semiempirical dispersion contributions were also included into DFT computations by means of the D3 model of Grimme,[37] leading to B3LYP-D3 and B2PLYP-D3 models.[38] Full geometry optimizations have been performed for both *anti* and *gauche* conformers checking the nature of the obtained structures by diagonalizing their Hessians. Cubic and semi-diagonal quartic force constants have been next computed by finite differences of analytical Hessians at the B3LYP and B3LYP-D3 levels and used to obtain anharmonic frequencies with the GVPT2 model taking into the proper account possible resonances for frequencies[15] together with IR and Raman intensities with the DVPT2 model including both mechanical and electrical anharmonicities.[18,19] All calculations have been performed in vacuum (except if noted) to be directly comparable to available experimental data and taking full account of symmetry in all computational steps including finite differentiations for obtaining cubic and quartic force constants. Torsional degrees of freedom have been treated by the hindered rotor (HR) approximation[16,17] extended to the anharmonic oscillator (HRAO) level.[39] Zero point energies (ZPE) and thermodynamic functions were evaluated by a resonance-free anharmonic model extended to include also hindered rotations.[18,39] All the spectra have been generated and managed by the VMS-draw graphical user interface.[22]

RESULTS AND DISCUSSION

Structure and Thermochemistry. The structures of DPE have been optimized enforcing C_{2h} (*anti*) and C_2 (*gauche*) symmetries with a high level of accuracy in order to minimize the numerical noise connected with numerical integration of exchange and correlation contributions. Of course, the largest difference between *anti* and *gauche* conformers is observed for the torsion angle around the central Csp^3-Csp^3 bond (ψ), whose optimized values are 180° and ≈65° for *anti* and *gauche* conformers, respectively (Tables 1 and 2). At the B3LYP/6-31+G(d) level the *anti* conformer is found more stable by 0.9 kcal·mol^{-1} and the value increases to about 1 kcal·mol^{-1} when the ZPE is taken into account (at both harmonic and anharmonic levels of theory). Furthermore, inclusion of thermal and entropic contributions further stabilizes the *anti* conformer with respect to its *gauche* counterpart. Also B2PLYP/m-aug-cc-pvtz computations found *anti* more stable than *gauche*, but this time, the energy difference is significantly smaller (0.16 kcal·mol^{-1}). However, as discussed in ref 9, both the optimal ψ torsional angle and the relative stability of the *gauche* conformer show a significant method and basis set dependence. For instance, MP2 computations strongly favor the gauche conformer (by more than 2 kcal·mol^{-1}). The trend of results is thus very similar to those obtained by Ivanov in his different studies.[8,9]

Table 1. Energy Differences (kcal·mol^{-1}) between *Anti* and *Gauche* Conformer vs Dihedral ψ_g Angle (deg) of *Gauche* and Level of Theory

	anti	*gauche*	$\lvert\Psi_g\rvert$ (deg)
B3LYP/6-31+G(d)	0.00	0.86	−68
B3LYP/m-aug-cc-pvtz	0.00	0.94	−68
MP2/m-aug-cc-pvtz	2.29	0.00	−58
B2PLYP/m-aug-cc-pvtz	0.00	0.16	−65
B3LYP-D3/m-aug-cc-pvtz	0.54	0.00	−64
B3LYP-D3/6-31+G(d)	0.64	0.00	−64
B2PLYP-D3/m-aug-cc-pvtz	0.72	0.00	−63
CCSD(T)/m-aug-cc-pvtz[a]	0.74	0.00	−65
B3LYP/6-31+G(d)/$CHCl_3$	0.00	0.93	−67
B3LYP-D3/6-31+ G(d)/$CHCl_3$	0.48	0.00	−63

[a]Energy computed on the optimized B2PLYP/m-aug-cc-pvtz geometry.

Therefore, this stability problem has been analyzed using the CCSD(T) model and adding the D3 empirical dispersion[37] in DFT computations. As shown in Table 1, when one includes dispersion effects, the *gauche* conformer becomes more stable than its *anti* counterpart by 0.5−0.7 kcal·mol^{-1} at both B3LYP-D3 and B2PLYP-D3 levels. CCSD(T) single-point computations at the m-aug-cc-pvtz level were next performed at B2PLYP/m-aug-cc-pvtz optimized geometries.

These computations show the same energetic trend as MP2 and DFT including dispersion effects (i.e., *gauche* is energetically more stable), and there is actually a quantitative

dx.doi.org/10.1021/ct500930b | J. Chem. Theory Comput. 2014, 10, 5586−5592

Table 2. Key Geometric Parameters of Bibenzyl Conformers (B3LYP-D3/6-31+G(d))

	Anti (C_{2h})	*Gauche* (C_2)	TS1 (C_2)	TS2 (C_{2v})
$C_{sp2}-C_{sp3}$ (Å)	1.512 1.513 (3)[a]	1.512	1.512	1.513
$C_{sp3}-C_{sp3}$ (Å)	1.551 1.529 (3)[a]	1.555	1.572	1.581
$C_{sp3}-C_{sp2}$ (Å)	1.512	1.512	1.512	1.513
$C_{sp2}-C_{sp3}-C_{sp3}$ (deg)	112.2 113.2 (2)[a]	112.9	112.9	115.9
χ (deg)	88.8/−88.8 65.3 (2)[a]	93.3/−83.9	90.1/−87.2	89.3/−89.3
φ (deg)	88.8/−88.8	93.3/−83.9	90.1/−87.2	89.3/−89.3
Ψ (deg)	180	±64	±123	0

[a]From ref 43 at 100 K.

agreement with B2PLYP-D3/m-aug-cc-pVTZ results ($\Delta E \approx$ 0.7 kcal·mol^{-1} in both cases). Furthermore, ZPE, thermal, and entropic contributions show very similar trends at both harmonic and HRAO levels, favoring the *anti* conformer by about 0.6 kcal·mol^{-1}. Taking into account these contributions to the most reliable electronic energy difference (0.7 kcal·mol^{-1} in favor of *gauche*), the statistical factors (2 vs 1 for *gauche* and *anti*, respectively), we end up with 70% for *gauche* and 30% for *anti* at 298 K.

To estimate the energy barrier from *anti* to *gauche* conformers, a relaxed scan has been performed at the B3LYP-D3/6-31+G(d) level of theory. As one can see in Figure 2, according to our computations, the interconversion of

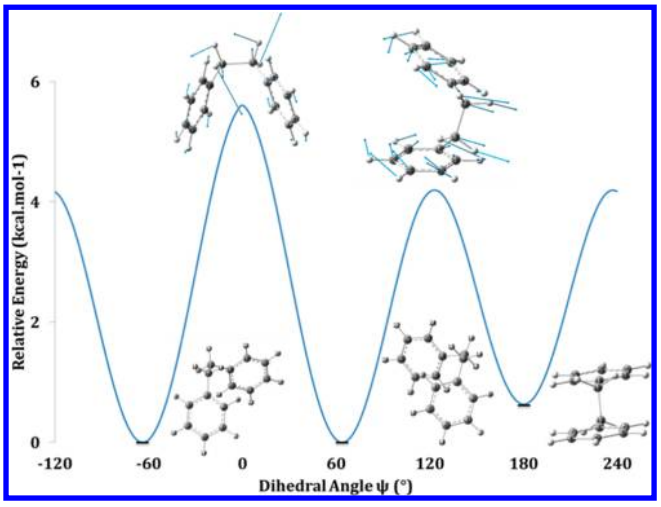

Figure 2. Flexible rotor potential energy profile along the ψ dihedral angle for bibenzyl in the gas phase (B3LYP-D3/6-31+G(d)).

the two *gauche* conformers is ruled by a saddle point of C_{2v} symmetry, which lies 5.6 kcal·mol^{-1} above *gauche* conformers ($\approx$ 100i cm^{-1}).

Furthermore, two transition states (with imaginary frequency of 42i cm^{-1}) have been found 4.2 kcal·mol^{-1} above the *gauche* minima, linking each of these conformers to the *anti* one.

The overall potential energy profile governing motion along the ψ torsional angle obtained in the flexible rotor approximation is shown in Figure 2.

Test computations employing the polarizable continuum model (PCM)[40−42] to take into account bulk solvent effects (chloroform) suggest that the situation should be essentially the same in solution (again in agreement with experiment), with an energetic behavior close to the ones obtained in the gas phase, whereas crystal-packing effects could lead to a more complex picture in the solid phase.

Infrared Spectra. On the grounds of the results discussed in the section above and of previous results,[44] B3LYP and B3LYP-D3/6-31+G* anharmonic computations have been performed to simulate the vibrational spectra (both IR and Raman) of bibenzyl.

As a starting point, in Figure 3 the experimental IR spectrum of bibenzyl is compared to harmonic computations for the *anti*

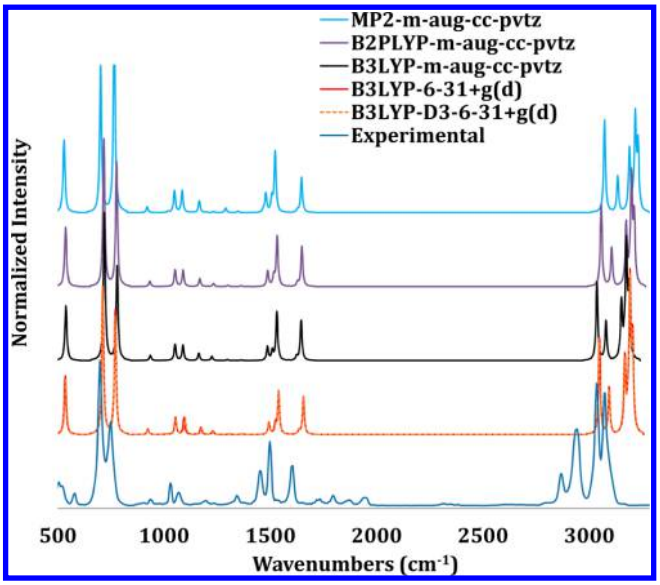

Figure 3. Observed (from ref 20) and simulated (*anti* conformer at different levels of theory) IR spectra of bibenzyl. Normalization has been performed with respect to the peak at ca. 700 cm^{-1}.

conformer. One can notice that, at this level of theory, all the positions of the peaks in the region 500−1000 cm^{-1} are nicely reproduced. The experimental peak at ca. 580 cm^{-1} was assigned to the *gauche* conformer;[14] therefore, it is absent in our simulations. In the region of 1000−2000 cm^{-1}, the most intense peaks are well reproduced in our computations but with a slight overall blue shift. Furthermore, the peak at ca. 1350 cm^{-1} was also assigned to the *gauche* conformer.[14] However, all the observed peaks in the range 1700−2000 cm^{-1} are absent in our computations, suggesting that they correspond to overtones or combination bands (see below). Finally, as expected, a stronger disagreement is obtained between experimental and

computed results concerning the peaks localized at the extreme of the mid-IR.

Turning now to IR intensities, Figure 3 shows that the peak with the highest observed intensity falls at about 700 cm^{-1}, and two other very intense peaks are found above 3000 cm^{-1}. The computed harmonic spectrum reproduces with difficulty this trend, with the most intense peak at ca. 3200 cm^{-1} instead of 700 cm^{-1}. To solve this issue, additional computations have been performed with a larger basis set (m-aug-cc-pvtz). As one can see, the peak at 700 cm^{-1} becomes the most intense one, in place of the one at 3200 cm^{-1}. With this basis set, B2PLYP and B3LYP intensities are quite similar, whereas the spectrum simulated at the MP2 level is rather different from the others. For instance, the most intense band now falls at 770 cm^{-1} instead of 700 cm^{-1}.

B3LYP/6-31+G(d) and B3LYP-D3/6-31+G(d) cubic and semidiagonal quartic force constants have been next computed by numerical differentiation of analytical Hessians obtaining, at the same time, the second and semidiagonal third derivatives of dipole moments and polarizabilities needed for including electric anharmonicity effects. These quantities have been used to perform GVPT2 and DVPT2 evaluations of anharmonic frequencies and intensities, respectively. In agreement with a previous report,[14] if the anharmonic treatment is performed without symmetry (B3LYP/6-31+G(d)), there is an imaginary frequency which appears for the *anti* conformer (from 22 cm^{-1} to *i*15 cm^{-1}, at the harmonic and anharmonic level, respectively) and not for the *gauche* one. However, when symmetry is properly taken into account in the perturbative treatment, the frequency remains real also at the anharmonic level (from 17 to 6 cm^{-1}), pointing out the problems of accuracy and of numerical instabilities inherent in numerical treatments. Furthermore, the slight difference of the computed lowest frequency between both cases (with or without symmetry) for *anti* conformer in DFT at the harmonic level does not appear when MP2 is used, suggesting that the problem is connected with the numerical integration of the exchange-correlation functional, whereas it is absent in fully analytical computations.

In Figure 4, the anharmonic spectra (B3LYP/6-31+G(d)) of *gauche* (green) and *anti* (red) conformers are shown, together with the experimental spectrum (blue). As one can see, some peaks can be assigned to one conformer or to the other without any doubt. For instance, the first and third peak at about 500 cm^{-1} can be assigned to the *gauche* conformer while the second one (*ca* 520 cm^{-1}) belongs more probably to the *anti* conformer.

Furthermore, the experimental peak around 1170 cm^{-1} is probably the result of an admixture of both conformers while the peak around 1340 cm^{-1} can be assigned to the *gauche* form. The global band shape is particularly well reproduced and the strongest effect of anharmonicity appears to be a huge increase of the intensity of the band at ≈3070 cm^{-1}. Furthermore, all the missing bands in the range 1700−2000 cm^{-1} are now well described in the simulated spectra. They correspond to multiple combination bands and overtones according to our predictions. Finally, with the exception of the very small peaks at ca. 2300 cm^{-1}, all the bands (and even shoulders) have been reproduced in our simulations. The computed spectrum obtained by using the populations of the two conformers discussed above (70% *gauche* and 30% *anti*) is reported in Figure 4 (broken line) and shows a remarkable agreement with experiment.

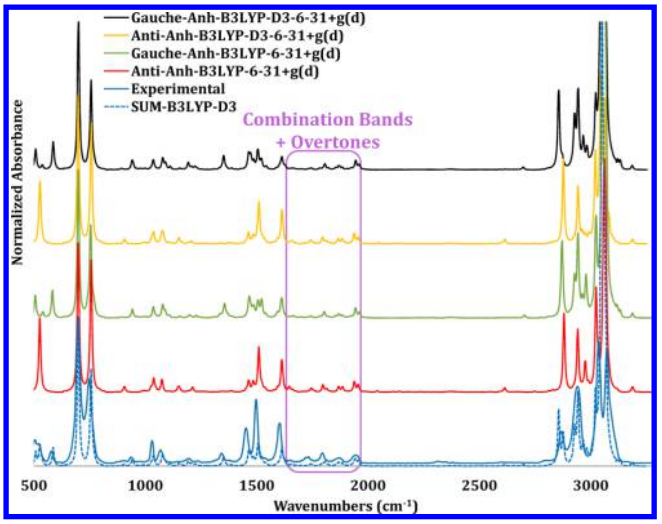

Figure 4. Experimental (blue) (from ref 20) and simulated anharmonic spectra of bibenzyl. Normalization has been performed with respect to the peak at ca. 700 cm^{-1}.

Raman Spectra. In order to gain further insights into the conformational and spectroscopic properties of DPE, Raman intensities have been computed for the *anti* conformer at both harmonic and anharmonic levels (B3LYP-D3/6-31+G(d)) and compared to the observed spectrum (in the liquid phase) in the 2800−3100 cm^{-1} region.[12] As one can see in Figure 5, the computed harmonic spectrum (red) displays only five peaks and there is a non-negligible disagreement for both wavenumbers and intensities. Furthermore, one should also notice

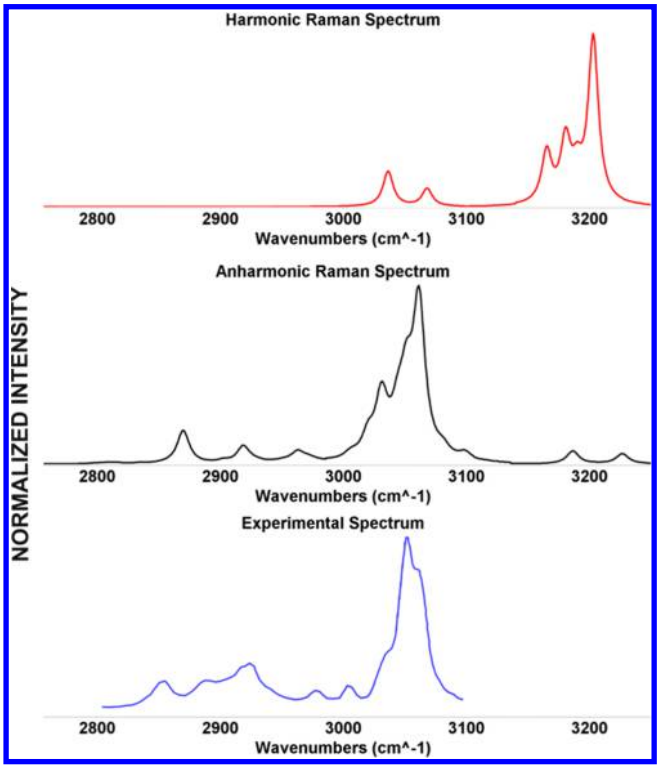

Figure 5. Experimental in liquid (blue, from ref 12) and computed *anti* conformer (red = harmonic, black = anharmonic) Raman spectra in the 2800−3200 cm^{-1} region (B3LYP-D3/6-31+G(d)). Spectra are normalized on the maximum of this wavenumber region.

dx.doi.org/10.1021/ct500930b | J. Chem. Theory Comput. 2014, 10, 5586−5592

that a lot of peaks are missing which confirms the need of an anharmonic treatment.

To be consistent with our infrared simulation, a full anharmonic Raman treatment has been performed. Contrary to its harmonic counterpart, the anharmonic spectrum (black) exhibits a good agreement with respect to experiment (blue) concerning the peak positions and also their intensities. Both strong peaks around 3060 cm^{-1} are presents at the anharmonic level, together with the shoulder at ca. 3040 cm^{-1}. Furthermore, the two peaks of the experimental spectrum around 3000 cm^{-1}, which were completely absent at the harmonic level, are fully reproduced at the anharmonic level.

A surprising result in our computations is the presence of only two peaks around 2900 cm^{-1} in place of the three observed ones. The missing peak at ∼2890 cm^{-1} could be the result of higher-level combination bands/set of overtones requiring more quanta in the anharmonic treatment or can be due to the presence of the *gauche* conformer in liquid phase. Another intriguing behavior concerns the intensities of the most intense peaks in this frequency region with respect to experiment (in solution). However, in a paper published in 1972 by Mathur et al.,[13] the intensity order between the two peaks at 3060 cm^{-1} is similar to the one obtained in our calculations, thus raising the question of the experimental conformer obtained in powder and in liquid phases. Therefore, we zoomed (Figure 6) the 3020−3080 cm^{-1} frequency region and compared the simulated spectra of *anti* and *gauche* conformers to the two observed ones. As one can see, the computed spectrum of the *anti* conformer is very similar to the second experimental spectrum (from ref[13]), which has been obtained for a crystalline powder, especially concerning the overall band-shape: the most intense peak in this region falls around 3060 cm^{-1}, and also the shoulder around 3055 cm^{-1} is well reproduced. The last small peak at 3040 cm^{-1} is only slightly red-shifted (at 3030 cm^{-1}) in our computations. All these results give further support to a prevalence of the *anti* conformer in the solid state.

On the contrary, the computed spectrum of the *gauche* conformer exhibits the same wavenumber and intensity trends as the experimental one in liquid phase (green), except for the peak at 3030 cm^{-1}, which could belong, according to our predictions, to the *anti* conformer. This last result confirms the difficulties in distinguishing both conformers in the liquid phase where, at the same time, *gauche* and *anti* forms have their own signatures in a small frequency region.

NMR. The B3LYP-D3/6-31+G(d) optimized structures in solution ($CHCl_3$) have been used to perform NMR computations in order to gain further insights about the conformational behavior of DPE in solution (Table 3). As one can see, the computed data for *gauche* and *anti* conformers are quite similar. The chemical shifts of sp^3 carbon atoms seem to be better reproduced by the *gauche* conformer. On the other hand, the computed chemical shifts range of the hydrogens on the phenyl moieties (H-φ) are in better agreement for the *anti* conformer than for the *gauche* one. These results give further support to the presence of both conformers in solution.

■ CONCLUDING REMARKS

We have performed a comprehensive analysis of the conformational behavior and spectroscopic characteristics of bibenzyl by latest generation quantum mechanical methods including anharmonic and hindered-rotor contributions. Although the energy difference between *anti* and *gauche* conformers is quite small, the most refined computations (CCSD(T) and dispersion-corrected DFT) agree in suggesting the contemporary presence of both species in the gas phase and in solution, with a predominance of the *gauche* conformer.

A second-order vibrational perturbative treatment has been able to provide remarkably accurate frequencies together with IR and Raman intensities provided that symmetry is properly taken into account, resonances are wisely managed, and conformational equilibria are accounted. Furthermore, as previously reported, use of extended basis sets can be mandatory at the harmonic level to obtain correct band shapes. Smaller basis sets can be, instead, confidently used to introduce

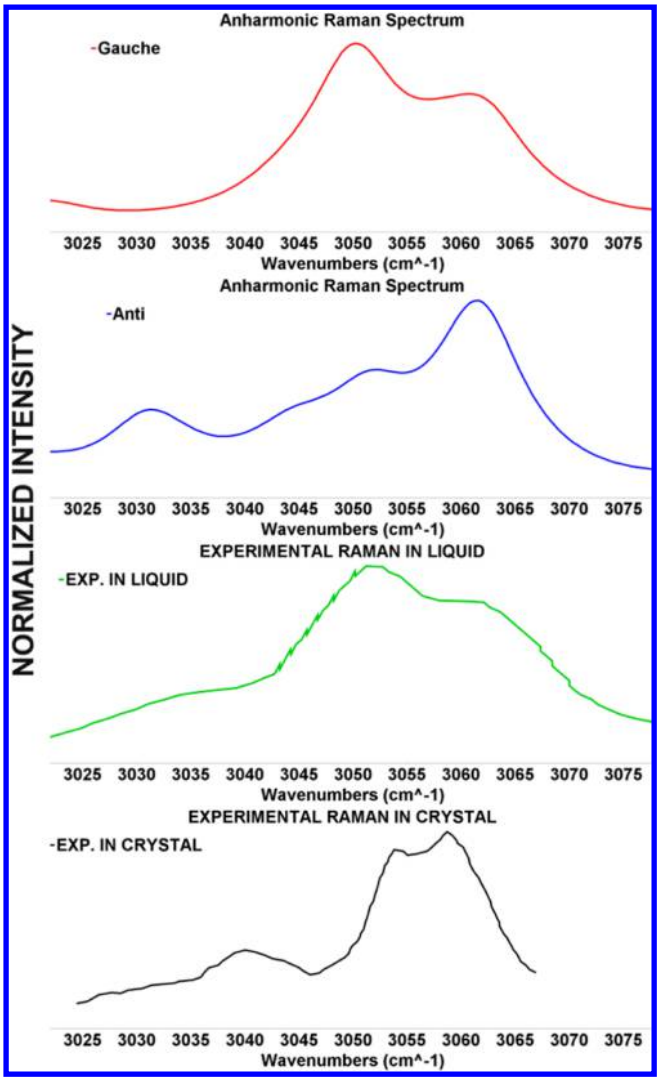

Figure 6. Experimental (liquid = green, crystal = black; from respectively refs 12 and 13) and simulated (red = *gauche*, blue = *anti*) Raman spectra in the 3020−3080 cm^{-1} region. Spectra are normalized on the maximum of this wavenumber region.

Table 3. Experimental (From Ref 45) and Computed Chemical Shifts (ppm) for *Anti* and *Gauche* Conformers in $CHCl_3$ (B3LYP-D3/6-31+G(d)/PCM)

	exp	*anti*	*gauche*
Csp3	38.10	46.65	42.97
H (Csp3)	3.07	2.75	2.64−3.15
Csp2	126−142	121−140	121−138
H-φ	7.31−7.44	7.31−7.46	6.24−7.44

dx.doi.org/10.1021/ct500930b | J. Chem. Theory Comput. 2014, 10, 5586−5592

anharmonic effects, again in agreement with previous suggestions.

This trend, already apparent for vibrational frequencies, is even more important for IR intensities and/or Raman activities,[19,46−50] where use of too small basis sets at the harmonic level can provide quite distorted spectral shapes. The most intense peak remains almost unchanged upon the anharmonic treatment, but some combination bands and overtones appear in the region 1700−2000 cm^{-1}, showing the importance of a proper inclusion of both mechanical and electrical anharmonicities.[18,19,51]

Finally, computation of NMR chemical shifts further confirms that, in agreement with experiment, both *anti* and *gauche* conformers can be observed at least in the gas phase and in solution.

Together with the intrinsic interest of the studied molecule, the implementation of all the building blocks of the used computational strategy in a widely distributed computer code paves the route toward full structural and spectroscopic characterization of large, flexible molecules both in the gas phase and in solution by means of integrated experimental and computational studies of unprecedented effectiveness and reliability.

■ ASSOCIATED CONTENT

Supporting Information

This material is available free of charge via the Internet at http://pubs.acs.org.

■ AUTHOR INFORMATION

Corresponding Author

*E-mail: vincenzo.barone@sns.it.

Notes

The authors declare no competing financial interest.

■ ACKNOWLEDGMENTS

The research leading to these results has received funding from the European Union's Seventh Framework Programme (FP7/2007-2013) under grant agreement No. ERC-2012-AdG-320951-DREAMS. The authors gratefully thank the high-performance computer facilities of the DREAMS center (http://dreamshpc.sns.it) for providing computer resources. The support of the COST CMTS-Action CM1002 "Convergent Distributed Environment for Computational Spectroscopy (CODECS)" is also acknowledged.

■ REFERENCES

(1) Hernández-Romero, Y.; Acevedo, L.; de Los Ángeles Sánchez, M.; Shier, W. T.; Abbas, H. K.; Mata, R. Phytotoxic Activity of Bibenzyl Derivatives from the Orchid *Epidendrum rigidum*. *J. Agric. Food Chem.* **2005**, *53*, 6276−6280.

(2) Chen, C.-C.; Wu, L.-G.; Ko, F.-N.; Teng, C.-M. Antiplatelet Aggregation Principles of *Dendrobium loddigesii*. *J. Nat. Prod.* **1994**, *57*, 1271−1274.

(3) Miyazawa, M.; Shimamura, H.; Nakamura, S.; Sugiura, W.; Kosaka, H.; Kameoka, H. Moscatilin from *Dendrobium nobile*, a Naturally Occurring Bibenzyl Compound with Potential Antimutagenic Activity. *J. Agric. Food Chem.* **1999**, *47*, 2163−2167.

(4) Baur, J. A.; Sinclair, D. A. Therapeutic Potential of Resveratrol: The In Vivo Evidence. *Nat. Rev. Drug Discovery* **2006**, *5*, 493−506.

(5) Barrero, A. F.; Herrador, M. M.; Quílez del Moral, J. F.; Arteaga, P.; Akssira, M.; El Hanbali, F.; Arteaga, J. F.; Diéguez, H. R.; Sánchez, E. M. Couplings of Benzylic Halides Mediated by Titanocene Chloride: Synthesis of Bibenzyl Derivatives. *J. Org. Chem.* **2007**, *72*, 2251−2254.

(6) Todd, R.; Rubio, G.; Hall, D. J.; Tempelaar, S.; Dove, A. P. Benzyl Bispidine as an Efficient Replacement for (−)-Sparteine in Ring Opening Polymerisation. *Chem. Sci.* **2013**, *4*, 1092−1097.

(7) Gardner, B. M.; Cleaves, P. A.; Kefalidis, C. E.; Fang, J.; Maron, L.; Lewis, W.; Blake, A. J.; Liddle, S. T. The Role of 5f-Orbital Participation in Unexpected Inversion of the σ-Bond Metathesis Reactivity Trend of Triamidoamine Thorium(IV) and Uranium(IV) Alkyls. *Chem. Sci.* **2014**, *5*, 2489−2497.

(8) Kurita, N.; Ivanov, P. M. Correlated Ab Initio Molecular Orbital (MP3, MP4) and Density Functional (PW91, MPW91) Studies on the Conformations of 1,2-Diphenylethane. *J. Mol. Struct.* **2000**, *554*, 183−190.

(9) Ivanov, P. M. The Torsional Energy Profile of 1,2-Diphenylethane: An Ab Initio Study. *J. Mol. Struct.* **1997**, *415*, 179−186.

(10) Shen, Q. The Molecular Structure of 1,2-Diphenylethane as Determined by Gas-Phase Electron Diffraction. *J. Mol. Struct.* **1998**, *471*, 57−61.

(11) North, A. M.; Pethrick, R. A.; Wilson, A. D. Infrared and Raman Studies of Phenyl Substituted Ethanes. *Spectrochim. Acta Part A Mol. Spectrosc.* **1974**, *30*, 1317−1327.

(12) Horn, A.; Klaeboe, P.; Jordanov, B.; Nielsen, C. J.; Aleksa, V. Vibrational Spectra, Conformational Equilibrium, and Ab Initio Calculations of 1,2-Diphenylethane. *J. Mol. Struct.* **2004**, *695−696*, 77−94.

(13) Mathur, M. S.; Weir, N. A. The Laser Raman and Infrared Spectra of Crystalline Dibenzyl. *J. Mol. Struct.* **1972**, *14*, 303−311.

(14) Martin-Drumel, M. A.; Pirali, O.; Falvo, C.; Parneix, P.; Gamboa, A.; Calvo, F.; Bréchignac, P. Low-Energy Vibrational Spectra of Flexible Diphenyl Molecules: Biphenyl, Diphenylmethane, Bibenzyl, and 2-, 3-, and 4-Phenyltoluene. *Phys. Chem. Chem. Phys.* **2014**, *16*, 22062−22072.

(15) Barone, V. Anharmonic Vibrational Properties by a Fully Automated Second-Order Perturbative Approach. *J. Chem. Phys.* **2005**, *122*, 14108.

(16) Ayala, P. Y.; Schlegel, H. B. Identification and Treatment of Internal Rotation in Normal Mode Vibrational Analysis. *J. Chem. Phys.* **1998**, *108*, 2314.

(17) McClurg, R. B.; Flagan, R. C.; Goddard, W. A., III The Hindered Rotor Density-of-States Interpolation Function. *J. Chem. Phys.* **1997**, *106*, 6675.

(18) Bloino, J.; Biczysko, M.; Barone, V. General Perturbative Approach for Spectroscopy, Thermodynamics, and Kinetics: Methodological Background and Benchmark Studies. *J. Chem. Theory Comput.* **2012**, *8*, 1015−1036.

(19) Barone, V.; Biczysko, M.; Bloino, J. Fully Anharmonic IR and Raman Spectra of Medium-Size Molecular Systems: Accuracy and Interpretation. *Phys. Chem. Chem. Phys.* **2014**, *16*, 1759−1787.

(20) NIST Webbook: IR-Bibenzyl. http://webbook.nist.gov/cgi/cbook.cgi?ID=C103297&Units=SI&Mask=80#IR-Spec (accessed Sept. 25, 2014).

(21) Barone, V.; Baiardi, A.; Biczysko, M.; Bloino, J.; Cappelli, C.; Lipparini, F. Implementation and Validation of a Multi-Purpose Virtual Spectrometer for Large Systems in Complex Environments. *Phys. Chem. Chem. Phys.* **2012**, *14*, 12404−12422.

(22) Licari, D.; Baiardi, A.; Biczysko, M.; Egidi, F.; Latouche, C.; Barone, V. VMS. *J. Comput. Chem.* DOI: 10.1002/jcc.23785.

(23) Frisch, M. J.; Trucks, G. W.; Schlegel, H. B.; Scuseria, G. E.; Robb, M. A.; Cheeseman, J. R.; Scalmani, G.; Barone, V.; Mennucci, B.; Petersson, G. A.; Nakatsuji, H.; Caricato, M.; Li, X.; Hratchian, H. R.; Izmaylov, A. F.; Bloino, J.; Zheng, G.; Sonnenberg, J. L.; Hada, M.; Ehara, M.; Toyota, K.; Fukuda, R.; Hasegawa, J.; Ishida, M.; Nakajima, T.; Honda, Y.; Kitao, O.; Nakai, H.; Vreven, T.; Montgomery, J. A., Jr.; Peralta, J. R.; Ogliaro, F.; Bearpark, M.; Heyd, J. J.; Brothers, E.; Kudin, K. N.; Staroverov, V. N.; Kobayashi, R.; Normand, J.; Raghavachari, K.; Rendell, A.; Burant, J. C.; Iyengar, S. S.; Tomasi, J.; Cossi, M.; Rega, N.; Millam, J. M.; Klene, M.; Knox, J. E.; Cross, J. B.; Bakken, V.; Adamo, C.; Jaramillo, J.; Gomperts, R.; Stratmann, R. E.; Yazyev, O.;

Austin, A. J.; Cammi, R.; Pomelli, C.; Ochterski, J. W.; Martin, R. L.; Morokuma, K.; Zakrzewski, V. G.; Voth, G. A.; Salvador, P.; Dannenberg, J. J.; Dapprich, S.; Daniels, A. D.; Farkas, O.; Foresman, J. B.; Ortiz, J. V; Cioslowski, J.; Fox, D. J. *Gaussian09*; Gaussian, Inc.: West Conshohocken, PA, 2014.

(24) Stephens, P. J.; Devlin, F. J.; Chabalowski, C. F.; Frisch, M. J. Ab Initio Calculation of Vibrational Absorption and Circular Dichroism Spectra Using Density Functional Force Fields. *J. Phys. Chem.* **1994**, *98*, 11623−11627.

(25) Lee, C.; Yang, W.; Parr, R. G. Development of the Colle−Salvetti Correlation-Energy Formula into a Functional of the Electron Density. *Phys. Rev. B* **1988**, *37*, 785−789.

(26) Becke, A. D. Density-Functional Thermochemistry. III. The Role of Exact Exchange. *J. Chem. Phys.* **1993**, *98*, 5648−5652.

(27) Hehre, W. J.; Ditchfield, R.; Pople, J. A. Self-Consistent Molecular Orbital Methods. XII. Further Extensions of Gaussian-Type Basis Sets for Use in Molecular Orbital Studies of Organic Molecules. *J. Chem. Phys.* **1972**, *56*, 2257−2261.

(28) Grimme, S. Semiempirical Hybrid Density Functional with Perturbative Second-Order Correlation. *J. Chem. Phys.* **2006**, *124*, 034108.

(29) Head-Gordon, M.; Head-Gordon, T. Analytic MP2 Frequencies without Fifth-Order Storage. Theory and Application to Bifurcated Hydrogen Bonds in the Water Hexamer. *Chem. Phys. Lett.* **1994**, *220*, 122−128.

(30) Frisch, M. J.; Head-Gordon, M.; Pople, J. A. Semi-Direct Algorithms for the MP2 Energy and Gradient. *Chem. Phys. Lett.* **1990**, *166*, 281−289.

(31) Frisch, M. J.; Head-Gordon, M.; Pople, J. A. A Direct MP2 Gradient Method. *Chem. Phys. Lett.* **1990**, *166*, 275−280.

(32) Sæbø, S.; Almlöf, J. Avoiding the Integral Storage Bottleneck in LCAO Calculations of Electron Correlation. *Chem. Phys. Lett.* **1989**, *154*, 83−89.

(33) Head-Gordon, M.; Pople, J. A.; Frisch, M. J. MP2 Energy Evaluation by Direct Methods. *Chem. Phys. Lett.* **1988**, *153*, 503−506.

(34) Pople, J. A.; Head-Gordon, M.; Raghavachari, K. Quadratic Configuration Interaction. A General Technique for Determining Electron Correlation Energies. *J. Chem. Phys.* **1987**, *87*, 5968.

(35) Papajak, E.; Leverentz, H. R.; Zheng, J.; Truhlar, D. G. Efficient Diffuse Basis Sets: cc-pV*x*Z+ and maug-cc-pV*x*Z. *J. Chem. Theory Comput.* **2009**, *5*, 1197−1202.

(36) Dunning, T. H. Gaussian Basis Sets for Use in Correlated Molecular Calculations. I. The Atoms Boron through Neon and Hydrogen. *J. Chem. Phys.* **1989**, *90*, 1007.

(37) Grimme, S.; Antony, J.; Ehrlich, S.; Krieg, H. A Consistent and Accurate Ab Initio Parametrization of Density Functional Dispersion Correction (DFT-D) for the 94 Elements H-Pu. *J. Chem. Phys.* **2010**, *132*, 154104.

(38) Goerigk, L.; Grimme, S. Efficient and Accurate Double-Hybrid-Meta-GGA Density Functionals—Evaluation with the Extended GMTKN30 Database for General Main Group Thermochemistry, Kinetics, and Noncovalent Interactions. *J. Chem. Theory Comput.* **2011**, *7*, 291−309.

(39) Barone, V.; Biczysko, M.; Bloino, J.; Puzzarini, C. Glycine Conformers: A Never-Ending Story? *Phys. Chem. Chem. Phys.* **2013**, *15*, 1358−1363.

(40) Tomasi, J.; Mennucci, B.; Cammi, R. Quantum Mechanical Continuum Solvation Models. *Chem. Rev.* **2005**, *105*, 2999−3094.

(41) Barone, V.; Cossi, M.; Tomasi, J. A New Definition of Cavities for the Computation of Solvation Free Energies by the Polarizable Continuum Model. *J. Chem. Phys.* **1997**, *107*, 3210.

(42) Cossi, M.; Scalmani, G.; Rega, N.; Barone, V. New Developments in the Polarizable Continuum Model for Quantum Mechanical and Classical Calculations on Molecules in Solution. *J. Chem. Phys.* **2002**, *117*, 43.

(43) Harada, J.; Ogawa, K.; Tomoda, S. The Central Bond Length in 1,2-Diphenylethanes. *J. Am. Chem. Soc.* **1995**, *117*, 4476−4478.

(44) Fornaro, T.; Biczysko, M.; Monti, S.; Barone, V. Dispersion Corrected DFT Approaches for Anharmonic Vibrational Frequency Calculations: Nucleobases and Their Dimers. *Phys. Chem. Chem. Phys.* **2014**, *16*, 10112−10128.

(45) NMR-C14H14, http://www.sciencesoft.net/1,2-diphenylethane/index.html (accessed Sept. 25, 2014).

(46) Halls, M. D.; Schlegel, H. B. Comparison of the Performance of Local, Gradient-Corrected, and Hybrid Density Functional Models in Predicting Infrared Intensities. *J. Chem. Phys.* **1998**, *109*.

(47) Halls, M. D.; Schlegel, H. B. Comparison Study of the Prediction of Raman Intensities Using Electronic Structure Methods. *J. Chem. Phys.* **1999**, *111*.

(48) Galabov, B.; Yamaguchi, Y.; Remington, R. B.; Schaefer, H. F. High Level Ab Initio Quantum Mechanical Predictions of Infrared Intensities. *J. Phys. Chem. A* **2002**, *106*, 819−832.

(49) Thomas, J. R.; DeLeeuw, B. J.; Vacek, G.; Crawford, T. D.; Yamaguchi, Y.; Schaefer, H. F. The Balance between Theoretical Method and Basis Set Quality: A Systematic Study of Equilibrium Geometries, Dipole Moments, Harmonic Vibrational Frequencies, and Infrared Intensities. *J. Chem. Phys.* **1993**, *99*.

(50) Cheeseman, J. R.; Frisch, M. J. Basis Set Dependence of Vibrational Raman and Raman Optical Activity Intensities. *J. Chem. Theory Comput.* **2011**, *7*, 3323−3334.

(51) Latouche, C.; Palazzetti, F.; Skouteris, D.; Barone, V. High Accuracy Vibrational Computations for Transition Metal Complexes Including Anharmonic Corrections: Ferrocene, Ruthenocene, and Osmocene as Test Cases. *J. Chem. Theory Comput.* **2014**, *10*, 4565−4573.